Viscous dissipation effects in entrance region heat transfer for a power law fluid flowing between parallel plates

S. Gh. Etemad, A. S. Mujumdar and B. Huang
Department of Chemical Engineering, McGill University, Montreal, Quebec, Canada

A numerical investigation was carried out to predict the simultaneously developing steady laminar flow and heat transfer to a purely viscous non-Newtonian fluid described by a power law model flowing between two parallel plates. Several different thermal boundary conditions were examined. It is shown that the Nusselt number distribution along the walls is affected appreciably by the variation of the fluid viscosity with temperature, viscous dissipation, the magnitude of the power law index as well as the fluid Prandtl number and thermal boundary conditions.

Keywords: simultaneously developing; parallel plates; forced convection; variable viscosity; viscous dissipation; boundary conditions

Introduction

Heat transfer to purely viscous non-Newtonian fluids is frequently encountered in various industries (e.g., chemical, petrochemical and food processing). These fluids are commonly processed under laminar flow conditions because of their high apparent viscosities and also the small hydraulic diameters employed in compact heat exchangers.

Several types of heat exchangers are now available for a wide variety of applications requiring excellent heat-transfer performance. Plate heat exchangers belong to this category. In many cases, because of the relatively short length of compact heat exchangers, the entrance region heat transfer and pressure drop are parameters of practical interest.

Two types of thermal boundary conditions are of primary interest: constant wall temperature, denoted here by T, and constant wall heat flux, denoted by H. Different combinations of these boundary conditions may be applicable in specific cases.

Simultaneously developing steady laminar flow and heat transfer for flows between parallel plates have been studied extensively. Shah and London (1978), Shah and Bhatti (1987) among others have published extensive compilations of available information, both experimental and computational. Huhn (1992) has correlated the data of various investigations and developed an empirical correlation for the entry length Nusselt number in such flows. However, to date, very few studies have been reported in the literature on the simultaneously developing region between parallel plates for non-Newtonian fluids. In an excellent literature review Hartnett and Kostic (1989) have summarized the investigations on heat transfer to power law fluids flowing in square ducts and parallel plates. A brief review of the most relevant studies is presented here.

Address reprint requests to Professor Mujumdar at the Department of Chemical Engineering, McGill University, 3480 University Street, Montreal, Quebec, Canada H3A 2A7.

Received 27 July 1993; accepted 16 November 1993

Yau and Tien (1963) employed the momentum and energy integral method of von Kármán and Pohlhausen to solve the laminar entrance heat-transfer problem for power law non-Newtonian fluids flowing between parallel plates for type T boundary condition. As noted by Hartnett and Kostic (1989) their Nusselt number predictions appear to be in error when recalculated on the basis of Nu_x versus X^*_{th} with the Prandtl number as the parameter. The numerical marching method of Patankar and Spalding (1970) was used by Lin (1977) and Lin and Shah (1978) for T-boundary condition. These investigations cover a wide range of power law index and Prandtl number values.

An important feature of most purely viscous non-Newtonian fluids is that some of their rheological and thermophysical properties are very sensitive to temperature. This variation can have a large effect on the development of the velocity and temperature profiles and consequently on the pressure drop and heat transfer rates. Lin and Hsu (1980) considered this problem for non-Newtonian fluids flowing between parallel plates for a fully developed velocity profile at the inlet. Klemp et al. (1992) applied a combined asymptotic and finite-difference method to account for the viscosity variation of purely viscous non-Newtonian fluids subjected to the H boundary condition. They presented results for both Reynolds number and Peclet numbers equal to 1.

The factor that plays a key role in the thermal control of some polymer processing operations is viscous dissipation. The first theoretical work considering viscous dissipation is credited to Brinkman (1951) who examined the flow in a capillary. The effect of viscous dissipation for thermally developing laminar flow of Newtonian and non-Newtonian fluids between parallel plates was studied recently by Flores et al. (1991). This effect for a simultaneously developing flow situation has not been considered heretofore.

Review of the existing literature reveals little work on the simultaneously developing entry-length problem for power law fluids flowing between horizontal parallel plates. The present work considers the effects of the power law index, temperature-dependent viscosity and viscous dissipation under a variety of constant temperature and constant heat flux wall boundary conditions.

Notation

B dimensionless temperature—viscosity coefficient defined by Equations 9 and 10

B' temperature-viscosity coefficient defined by Equation 2

Br Brinkman number $\left(= \dfrac{k_0 u_e^{n+1}}{K(T_e - T_w)D_h^{n-1}}\right.$ for T-type and $\left. = \dfrac{k_0 u_e^{n+1}}{D_{hq}^n}\right.$ for H-type boundary conditions$\Big)$

C defined by Equation 7

C_p heat capacity

D defined by Equation 7

D_h hydraulic diameter ($=2H$)

E defined by Equation 7

f friction factor $\left(= \dfrac{\tau_w}{\frac{1}{2}\rho u_e^2}\dfrac{1}{4X}\right)$

f_{app} apparent friction factor

$f(T)$ temperature dependence function of the consistency index defined by Equation 2

$F(\theta)$ dimensionless temperature dependence function of the consistency index defined by Equations 9 and 10

g gravity acceleration

H channel height

K thermal conductivity

k_0 consistency index at reference temperature ($=T_w$ for T-type and $= T_e$ for H-type boundary conditions)

n power law index

Nu_H fully developed Nusselt number for H boundary condition

$Nu_{H(1)}$ fully developed Nusselt number for H(1) boundary condition

Nu_l local Nusselt number based on the temperature difference between the wall and the inlet fluid

Nu_m mean Nusselt number $\left(= \dfrac{1}{X}\displaystyle\int_0^X Nu_x dX\right)$

Nu_T fully developed Nusselt number for T boundary condition

$Nu_{T(1)}$ fully developed Nusselt number for T(1) boundary condition

Nu_x local Nusselt number $\left(= \dfrac{\left(\frac{\partial\theta}{\partial Y}\right)_w}{\theta_w - \theta_b}\right.$ for H-type and $\left. = \dfrac{\left(\frac{\partial\theta}{\partial Y}\right)_w}{\theta_b}\right.$ for T-type boundary conditions$\Big)$

p pressure

P dimensionless pressure $\left(= \dfrac{p - \rho g y}{\rho u_e^2}\right)$

Δp axial pressure drop ($= p_e - p$)

Pe Peclet number $\left(= \dfrac{\rho C_p u_e D_h}{K}\right)$

Pr Prandtl number $= \dfrac{k_0 C_p \left(\frac{u_e}{D_h}\right)^{n-1}}{K}$

q heat flux

Q_x dimensionless heat flux $\left(= \dfrac{q}{q|_{Y=0}}\right)$

Re Reynolds number $\left(= \dfrac{\rho u_e^{2-n} D_h^n}{k_0}\right)$

T temperature

u axial velocity

U dimensionless axial velocity $\left(= \dfrac{u}{u_e}\right)$

U_c dimensionless centerline velocity

v transverse velocity

V dimensionless transverse velocity $\left(= \dfrac{v}{u_e}\right)$

x axial distance

X dimensionless axial distance $\left(= \dfrac{x}{D_h}\right)$

X^*_{hy} dimensionless axial coordinate $\left(= \dfrac{x}{D_h Re}\right)$

X^*_{th} dimensionless axial coordinate $\left(= \dfrac{x}{D_h Pe}\right)$

y transverse distance

Y dimensionless transverse distance $\left(= \dfrac{y}{D_h}\right)$

Greek letters

Δ rate of deformation tensor in Cartesian coordinates

θ dimensionless temperature $\left(= \dfrac{T - T_w}{T_e - T_w}\right.$ for T-type and $\left. = \dfrac{T - T_e}{\frac{qD_h}{K}}\right.$ for H-type boundary conditions$\Big)$

$\theta_{b,x}$ dimensionless bulk temperature evaluated at x-axial position

ρ density

τ shear stress tensor

τ_w wall shear stress

Subscripts

b evaluated at bulk condition

e evaluated at inlet condition

H, x evaluated at local x-position for H-type boundary conditions

m mean value

T, m mean value evaluated at local x-position for T-type boundary conditions

T, x evaluated at local x-position for T-type boundary conditions

x evaluated at local x-position

w evaluated at wall condition

Problem statement

Figure 1 describes the basic flow configuration modeled. All fluid properties are taken to be constant except viscosity. The duct walls are held at either a fixed temperature or a constant heat flux. Further, combinations of these two classical boundary conditions were also examined (Table 1).

The power law model in its general form is

$$\tau = k_0 f(T)|\Delta{:}\Delta|^{n-1/2}\Delta \tag{1}$$

where n is the power law index ($n < 1$ pseudoplastic, $n = 1$ Newtonian and $n > 1$ dilatant behavior), k_0 is the consistency index at a reference temperature (T_0), and $f(T)$ gives the temperature dependence of the consistency index as follows:

$$f(T) = e^{B'(T-T_0)} \tag{2}$$

Here B' is an empirical constant (temperature-viscosity coefficient). The dimensionless forms of the applicable equations of continuity, momentum and energy are

Continuity:

$$\frac{\partial U}{\partial X} + \frac{\partial V}{\partial Y} = 0 \tag{3}$$

x-Momentum:

$$U\frac{\partial U}{\partial X} + V\frac{\partial U}{\partial Y} = -\frac{\partial P}{\partial X} + \frac{1}{\mathrm{Re}}\left(\frac{\partial C}{\partial X} + \frac{\partial D}{\partial Y}\right) \tag{4}$$

y-Momentum:

$$U\frac{\partial V}{\partial x} + V\frac{\partial V}{\partial Y} = -\frac{\partial P}{\partial Y} + \frac{1}{\mathrm{Re}}\left(\frac{\partial D}{\partial X} + \frac{\partial E}{\partial Y}\right) \tag{5}$$

Energy:

$$U\frac{\partial \theta}{\partial X} + V\frac{\partial \theta}{\partial Y} = \frac{1}{\mathrm{Pe}}\left(\frac{\partial^2\theta}{\partial X^2} + \frac{\partial^2\theta}{\partial Y^2}\right) + \frac{\mathrm{Br}}{\mathrm{Pe}} \times \left[C\frac{\partial U}{\partial X} + E\frac{\partial V}{\partial Y} + D\left(\frac{\partial U}{\partial Y} + \frac{\partial V}{\partial X}\right)\right] \tag{6}$$

where

$$C = 2\left\{2\left[\left(\frac{\partial U}{\partial X}\right)^2 + \left(\frac{\partial V}{\partial Y}\right)^2\right] + \left(\frac{\partial U}{\partial Y} + \frac{\partial V}{\partial X}\right)^2\right\}^{n-1/2}\frac{\partial U}{\partial X}F(\theta)$$

$$D = \left\{2\left[\left(\frac{\partial U}{\partial X}\right)^2 + \left(\frac{\partial V}{\partial Y}\right)^2\right] + \left(\frac{\partial U}{\partial Y} + \frac{\partial V}{\partial X}\right)^2\right\}^{n-1/2} \times \left(\frac{\partial U}{\partial Y} + \frac{\partial V}{\partial X}\right)F(\theta)$$

$$E = 2\left\{2\left[\left(\frac{\partial U}{\partial X}\right)^2 + \left(\frac{\partial V}{\partial Y}\right)^2\right] + \left(\frac{\partial U}{\partial Y} + \frac{\partial V}{\partial X}\right)^2\right\}^{n-1/2} \times \frac{\partial V}{\partial Y}F(\theta) \tag{7}$$

The dimensionless variables and dimensionless parameters in the preceding equations are defined as follows:

$$U = \frac{u}{u_e},\ V = \frac{v}{u_e},\ X = \frac{x}{D_h},\ Y = \frac{y}{D_h},\ P = \frac{p - \rho g y}{\rho u_e^2}$$

$$\mathrm{Re} = \frac{\rho u_e^{2-n} D_h^n}{k_0},\quad \text{and}\quad \mathrm{Pr} = \frac{k_0 C_p\left(\frac{u_e}{D_h}\right)^{n-1}}{K} \tag{8}$$

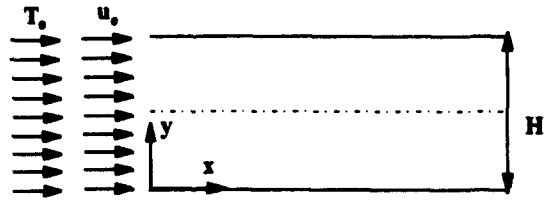

Figure 1 Channel geometry and inlet conditions

Table 1 Definition of the different thermal boundary conditions employed in the present study

Symbol	Geometry	Description	Boundary conditions
T	T_w / T_w	Constant temperature at both walls	$X=0$: $U=1$, $V=0$, $\theta=1$; $Y=0$ or $Y=0.5$: $U=0$, $V=0$, $\theta=0$
T(1)	insulated / T_w	Constant temperature at one wall; other wall insulated	$X=0$: $U=1$, $V=0$, $\theta=1$; $Y=0$: $U=0$, $V=0$, $\theta=0$; $Y=0.5$: $U=0$, $V=0$, $Q=0$
H	q / q	Constant heat flux at both walls	$X=0$: $U=1$, $V=0$, $\theta=0$; $Y=0$ or $Y=0.5$: $U=0$, $V=0$, $Q=1$
H(1)	insulated / q	Constant heat flux at one wall; other wall insulated	$X=0$: $U=1$, $V=0$, $\theta=0$; $Y=0$: $U=0$, $V=0$, $Q=1$; $Y=0.5$: $U=0$, $V=0$, $Q=0$

For the constant wall temperature boundary conditions we define

$$\theta = \frac{T - T_w}{T_e - T_w};\ \mathrm{Br} = \frac{k_0 u_e^{n+1}}{D_h^{n-1}(T_e - T_w)K};\ F(\theta) = e^{B'\theta(T_e - T_w)} = e^{B\theta},$$

$$\mathrm{Nu}_x = \frac{\left(\frac{\partial\theta}{\partial Y}\right)_{Y=0}}{\theta_b} \quad \text{and} \quad \mathrm{Nu}_x = \frac{-\left(\frac{\partial\theta}{\partial Y}\right)_{Y=1/2}}{\theta_b} \tag{9}$$

For constant heat flux boundary conditions the definitions are modified to

$$\theta = \frac{\dfrac{T - T_e}{qD_h}}{\dfrac{K}{}}; \quad \mathrm{Br} = \frac{k_0 u_e^{n+1}\left(\dfrac{1}{D_h}\right)^n}{q}; \quad F(\theta) = e^{B'\theta q D_h/K} = e^{B\theta}, \qquad (10)$$

$$\mathrm{Nu}_x = \frac{-\left(\dfrac{\partial\theta}{\partial Y}\right)_{Y=0}}{\theta_w - \theta_b} \quad \text{and} \quad \mathrm{Nu}_x = \frac{\left(\dfrac{\partial\theta}{\partial Y}\right)_{Y=1/2}}{\theta_w - \theta_b}$$

The dimensionless axial distance X^*_{th} is defined as

$$X^*_{th} = \frac{X}{\mathrm{RePr}} = \frac{X^*_{hy}}{\mathrm{Pr}} \qquad (11)$$

The Fanning friction factor, f, is defined as the ratio of the local wall shear stress to the fluid kinetic energy per unit volume. For a fully developed flow

$$f = \frac{\tau_w}{\frac{1}{2}\rho u_e^2} = \frac{\Delta p}{\frac{1}{2}\rho u_e^2}\frac{1}{4X} \qquad (12)$$

In the entrance region f is often called the apparent friction factor, f_{app}, and is based on the total pressure drop over axial position (from $X = 0$ to $X = X$). It takes into account both the skin friction and the change in shape of the velocity profile from the inlet.

The local dimensionless bulk temperature at each axial location (used in Equations 9 and 10) is calculated as follows:

$$\theta_{b,x} = \frac{\int_0^H \theta U dY}{\int_0^H U dY} \qquad (13)$$

The mean Nusselt number over length X measured from the inlet is given by

$$\mathrm{Nu}_m = \frac{1}{X}\int_0^X \mathrm{Nu}_x\, dX \qquad (14)$$

The heat flux is nondimensionalized in terms of the lower plate heat flux, ($Q_x = q/q\,|_{Y=0}$).

The boundary conditions for the four cases studied are shown in Table 1. Because of the long length of the plates (120 times of the hydraulic diameter) and also the high Peclect number (500–5,000) and relatively high Reynolds number values (500), a fully developed condition could be prescribed at the outlet boundary.

Equations 3–6 subjected to the different boundary conditions shown in Table 1 were solved using the fluid dynamic analysis package (based on the Galerkin finite element method). The Galerkin finite element method is well documented in the literature (e.g., Zienkiewicz 1977; Pittman 1989).

Results and discussion

The flow domain was descritized into 33 × 121 grids of 9-node quadratic quadrilateral elements, and penalty approach was chosen for the pressure with the penalty parameter set at 10^{-9}. Because of the higher velocity and temperature gradients in the entrance region and in the vicinity of the walls, finer mesh distributions were used in these regions. The combination strategy used to solve the algebraic equations starts with the fixed iteration method with a high relaxation factor for the initial iterations and then switches to the quasi–Newton-Raphson method with a smaller relaxation factor, thus resulting in a significant savings in computational time. Numerical stability of the solution was improved employing the Petrov-Galerkin formulation (streamline upwinding). The solution and the residual vectors were used as the criteria for convergence. Convergence is attained when the relative difference between successive solution vectors and the relative residual are each less than a specified tolerance. In this study the tolerance level of 10^{-5} was chosen for both convergence criteria. Using such combination convergence criteria provides a high level of accuracy of the solution vector.

To validate the numerical code the computed results were compared with the existing experimental results as well as available exact solutions. For the fully developed condition the centerline velocity and friction factor obtained from this study and the analytical results from the equations derived by Skelland (1967) were found to be in very close agreement (Table 2). The Nusselt numbers for hydrodynamically and thermally fully developed conditions are given in Table 3. For all boundary conditions, the present Nusselt numbers fell within 0.015 percent of the exact solution values.

The constant wall temperature boundary conditions [T and T(1)] were investigated by Mercer et al. (1967) using an interferometer. Figure 2 shows a comparison of the present results and their experimental data obtained for air. Again, the agreement is found to be excellent in the light of the experimental uncertainties. Note that the local Nusselt number defined by Mercer et al. is based on the temperature difference between the wall and the inlet fluid. For Figure 2, our results were calculated according to the Mercer et al. definition, although in the rest of this work the local Nusselt number is based on the temperature difference between the wall and the local fluid mixing cup temperature.

Table 4 compares the results from this study and those obtained by Hwang (1973, personal communication), and Hwang and Fan (1964) using a finite-difference method for Newtonian fluids. They employed this technique to obtain velocity distributions and then numerically integrated the

Table 2 Comparison between the U_c and f Re for parallel plates obtained from this investigation and earlier analytical calculations

		U_c	f Re
$n = 0.5$	Present work	1.327	7.99
	Analytical*	1.333	8.00
$n = 1.0$	Present work	1.491	23.88
	Analytical*	1.5	24.00
$n = 1.25$	Present work	1.546	40.69
	Analytical*	1.555	40.98

* Adapted from Skelland, A. H. P. 1967. *Non-Newtonian Flow and Heat Transfer.* Wiley, New York

Table 3 Comparison between the fully developed Newtonian Nusselt numbers for parallel plates obtained from the present investigation and analytical calculations for different boundary conditions (Ref. 18)

	$\mathrm{Nu}_{T(1)}$	Nu_T	$\mathrm{Nu}_{H(1)}$	Nu_H
Present work	4.8616	7.5410	5.3856	8.2353
Shah and London (1978)	4.8610	7.5407	5.3850	8.2353

Table 4 Comparison of Nusselt numbers reported by various researchers for Pr = 10, $n = 1$ and Re = 500

	$Nu_{T,m}$				$Nu_{T,x}$		$Nu_{H,x}$	
X^*_{th}	Nguyen and Maclaine-Cross (1991)	Hwang (1973)	Rostami and Mortazavi (1990)	Present work	Campos Silva et al. (1992)	Present work	Hwang and Fan (1964)	Present work
0.000125	—	46.68	47.46	47.18	27.75	24.72	34.07	34.24
0.000438	—	27.88	27.63	26.99	16.80	15.82	20.66	20.92
0.00075	—	21.94	22.28	21.76	13.70	13.34	17.03	17.18
0.0020	13.96	15.44	15.63	15.31	10.10	10.27	12.60	12.58
0.00625	10.49	11.01	11.33	10.95	8.20	8.15	9.50	9.51
0.010	9.54	9.86	10.4	9.80	7.79	7.72	8.80	8.76
0.0125	9.15	9.40	10.14	9.38	7.70	7.63	—	8.55
0.0250	8.42	8.47	—	8.41	7.56	7.55	—	8.26
0.0406	8.05	8.11	—	8.09	7.54	7.54	—	8.24

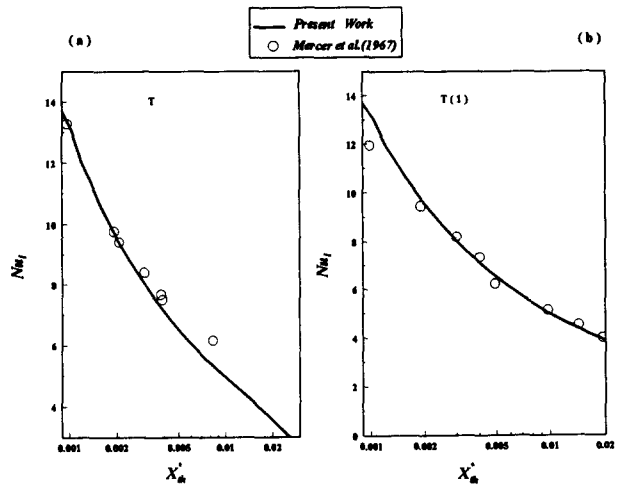

Figure 2 Comparison of the local Nusselt number with experimental data for Pr = 0.7 and $n = 1.0$

energy equation for both T and H boundary conditions; their Prandtl number values ranged from 0.01–50. These results were given by Shah and London (1978) and were claimed by Shah and Bhatti (1987) to be more accurate than other literature values. Nguyen (1991) also used a finite-difference method to solve the momentum and energy equations using the stream function as an independent variable. The results cover a wide range of Prandtl numbers (0.2–2,000).

This problem was also investigated analytically by Rostami and Mortazavi (1990) using a linear profile for the axial component of the velocity and solving the energy equation by the similarity method. They obtained a closed form expression for the Nusselt number as a function of X^*_{th} and the Prandtl number. This method is less applicable for low Prandtl numbers, because the assumption that a linear velocity profile in the thermal boundary layer introduces further errors. Their results show good agreement with the present investigation except in the downstream region where large discrepancies are due to the linear velocity profile assumption. The values of $Nu_{T,x}$ obtained by Campos Silva et al. (1992) are also tabulated in Table 4. They employed a linearization procedure for the flow problem and solved the decoupled energy equation using the generalized integral transform technique. Results were given for Pr = 0.72 and 10. Far downstream their results are comparable with the present study but close to the entrance the differences appear to be higher probably because of the specific linearization method they used which ignores the transverse velocity component in the developing flow region.

Table 5 compares the Nusselt numbers obtained in the present investigation and those reported by Lin (1977) for a non-Newtonian fluid ($n = 0.5$) at different Prandtl numbers (Pr = 1 and Pr = 10). This comparison shows very good agreement in the entire channel.

The Nusselt number under the constant heat flux conditions is higher than that under the constant wall temperature boundary condition ($Nu_{H,x} > Nu_{T,x}$) (Figure 3). The physical reason for this behavior can be developed from the consideration of the temperature profile. In the case of constant temperature boundary condition the temperature of the wall is constant and the fluid bulk temperature catches up with it, but for the constant heat flux boundary conditions the wall temperature is continuously moving away from the bulk temperature. Thus, for the same temperature difference between the wall and the fluid bulk, the temperature gradient of the fluid at the wall is smaller for the T boundary conditions because of the fact that the fluid close to the wall approaches the same temperature at the wall. Consequently the Nusselt numbers are lower for the T boundary conditions.

Generally for T-type boundary conditions the temperature difference of the bulk and the wall is one of the main factors for heat transfer. For T and T(1) boundary conditions, in the entrance region the differences between the bulk and wall temperatures are the same for heating walls, that is, the local Nusselt number based on the lower plate for T is very close to that for T(1). As the fluid proceeds downstream the

Table 5 Comparison of $Nu_{T,x}$ for $n = 0.5$ and Re = 500

Pr = 10			Pr = 1		
X^*_{th}	Lin (1977)	Present work	X^*_{th}	Lin (1977)	Present work
0.0007814	15.21	14.83	0.000609	20.71	20.97
0.0009989	13.86	13.59	0.001102	16.57	15.98
0.0012052	13.29	12.76	0.002173	12.29	12.12
0.0018029	11.43	11.28	0.004045	9.87	9.86
0.0023350	10.6	10.52	0.005712	9.05	9.03
0.0040173	9.29	9.29	0.010465	8.27	8.20
0.0060257	8.65	8.64	0.020552	8.00	7.97
0.0101102	8.21	8.14	0.026533	7.96	7.95
0.0205247	7.94	7.95			

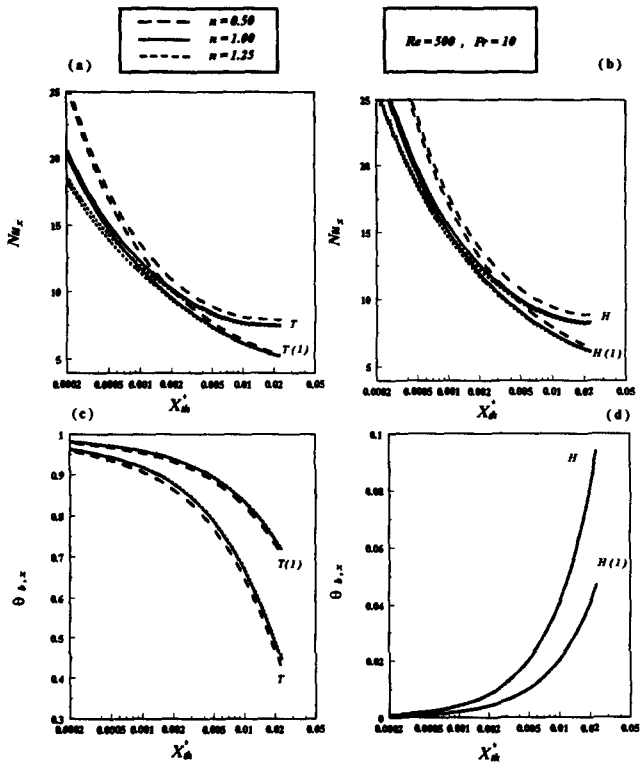

Figure 3(a–d) Effect of power law index on local Nusselt number and dimensionless bulk temperature for different boundary conditions

dimensionless bulk temperature for the T boundary condition decreases (the bulk temperature either increases, when $T_e < T_w$, or decreases, when $T_e > T_w$) more rapidly than that for the boundary condition T(1) and also the dimensionless heat flux for the T boundary condition decreases slightly more than that for T(1). These effects translate into a higher Nusselt number for the T boundary condition (Figure 3).

In the inlet region the bulk temperature as well as the wall temperature for H and H(1) boundary conditions are very close together. Farther downstream ($T_{w,x} - T_{b,x}$) for H is smaller than that for H(1) because of the heating at both walls for the H boundary condition. Therefore Nu_x for the H(1) boundary condition decreases over the axial distance more than that for H.

Effect of power law index

For the case of constant fluid viscosity, the dimensionless velocity profiles at different axial locations as well as U_{max} and f_{app} Re are demonstrated in Figures 4a–d for different values of n. For the same value of shear rate and consistency index the apparent viscosity for a pseudoplastic fluid is lower than that for a shear-thickening fluid. In the entrance of the duct, because of the viscous effects close to the walls and the high shear rate in the wall region, the velocity of the pseudoplastic fluid is higher than that of a dilatant fluid. Requirement of mass conservation forces the fluids to correspondingly slow down in the core of the duct. Farther downstream, viscous effects propagate to the centerplane of the channel and influence of the power law index diminishes. Figures 4c–d shows the centerline velocity and apparent friction factor decrease with decreasing the power law index.

Figures 3a–d shows the local Nusselt number and dimensionless bulk temperature distributions for different power law indices and also for various boundary conditions. As is shown the Nusselt number increases with decreasing n because of the steeper velocity gradient in the wall region for lower n values. Farther downstream this difference decreases. For the H boundary condition, $\theta_{b,x}$ is not affected noticeably by n. The reason is that the heat flux is the same for different power law index; therefore, difference in velocity profiles for different n's is not reflected in the bulk temperature.

For type T boundary condition the highest ($T_w - T_{b,x}$) as well as the velocity gradient at the wall exist in the entrance region, both decreasing monotonically with downstream distance. Conversely, for the constant heat flux boundary condition ($T_{w,x} - T_{b,x}$) is the smallest in the inlet region and increases with downstream distance, whereas the velocity gradient remains the highest at $X = 0$. The value of Nu_x is therefore determined by the counteracting influence of these two factors. Comparison between the Nusselt numbers for T and T(1) and also between H and H(1) boundary conditions shows the very small deviation in the relative enhancement of the Nusselt number in the entrance region because of a reduction in n. Far downstream the relative increase in velocity gradient close to the wall for smaller values of n diminishes but ($T_w - T_{b,x}$) for T decreases more than that for T(1) [and also ($T_{w,x} - T_{b,x}$) increases for H more than that for H(1)]. These effects cause a greater relative enhancement in Nu_x for T in comparison with T(1) and for H in comparison with H(1) in the region far from the inlet.

Effect of variable apparent viscosity

For most liquids the apparent viscosity decreases with increasing temperature. Therefore for heating $B > 0$ for T and T(1) boundary conditions, and $B < 0$ for H and H(1) boundary conditions.

Figures 5a–d show the effect of variable viscosity on the dimensionless velocity profile for various boundary conditions. Also, the effect of variable viscosity on the centerline velocity

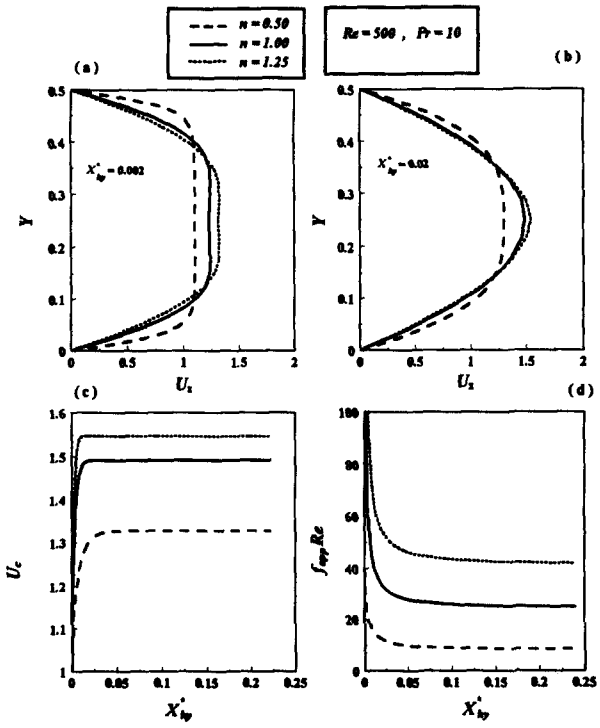

Figure 4(a–d) Effect of power law index on dimensionless velocity profile and friction factor and centerline velocity

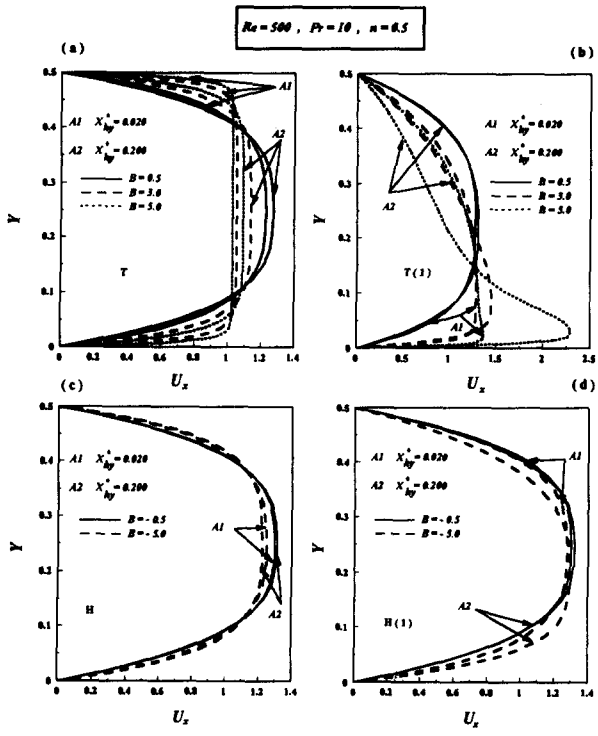

Figure 5(a–d) Effect of variable viscosity on dimensionless velocity profiles for different boundary conditions

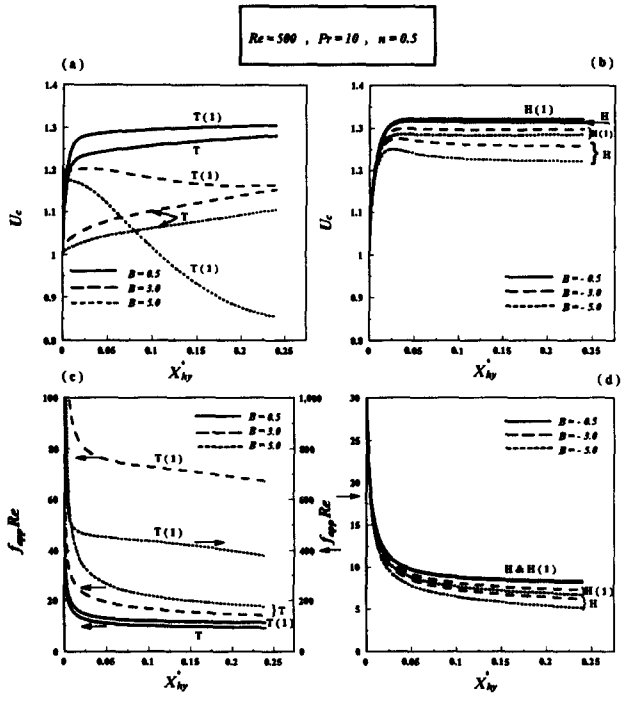

Figure 6(a–d) Effect of variable viscosity on centerline velocity and friction factor for different boundary conditions

and the apparent friction factor are demonstrated in Figures 6a–d.

In the case of heating, for both T- and H-type boundary conditions, increasing the temperature in the wall region decreases the apparent viscosity of the fluid in this region, resulting in higher velocity gradients near the wall and hence lower centerline velocities, which lead to enhanced heat transfer.

The effect of variable viscosity on the Nusselt number and the dimensionless bulk temperature for different boundary conditions can be seen from Figures 7a–d. This effect is not the same for different boundary conditions. For T and T(1) boundary conditions the temperature difference between the bulk and the wall is very large at the entrance, leading to large effect of variable viscosity in this region. The distortion of the temperature profile owing to the variation of viscosity with temperature is also significant. Farther downstream this difference decreases gradually, thus retarding the effect of variable viscosity.

The effect of temperature-dependent apparent viscosity on heat transfer is not as noticeable for the constant heat flux type boundary conditions as it is for the constant wall temperature situations. For H-type boundary conditions ($T_{w,x} - T_{b,x}$) is small in the entrance region and increases gradually in the axial direction. Thus the effect of variable viscosity on the velocity profile is small because the velocity profile is already developed (Figures 5c–d). Therefore, the enhancement of heat transfer is small relative to that for T-type boundary conditions. As is shown from Figure 7 the Nusselt number increases as B increases for T-type boundary conditions and also as B decreases for type H boundary conditions.

From Figure 5 it is easy to see that the distortion of the velocity profile for T(1) boundary condition is greater than that for the other boundary conditions. This results in greater relative enhancement (because of the temperature dependence of the consistency index) in the Nusselt number. Also, for the same reason the relative enhancement of the Nusselt number for H(1) is greater than that for H boundary condition.

In the case of variable apparent viscosity for non-Newtonian fluids the heat transfer rate is influenced by two factors: the

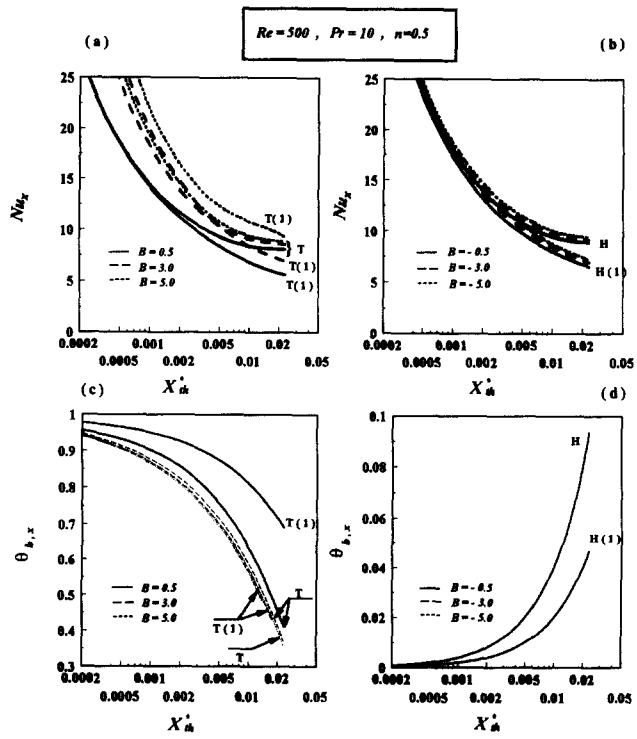

Figure 7(a–d) Effect of variable viscosity on the local Nusselt number and dimensionless bulk temperature for different boundary conditions

non-Newtonian behavior and the change in velocity profile owing to temperature-dependent apparent viscosity, which shows the importance of velocity gradient close to the wall for both cases. Comparison of Figures 3 and 7 indicates that the temperature dependence of the consistency index can have greater influence on the heat transfer rate than the power law index for T-type boundary conditions.

One important criterion in obtaining the constant viscosity solution is the selection of the temperature at which this viscosity should be evaluated. This reference temperature for T-type boundary conditions is chosen to be the temperature of the wall. Because the average viscosity in the momentum boundary layer is higher than that in the isoviscous case (based on the wall temperature as a reference) the pressure drop (and consequently the apparent friction factor) is higher for the variable viscosity case (Figure 6). Further, the inlet fluid temperature is used as the reference temperature to evaluate viscosity for H-type boundary conditions. Therefore, for heating, considering the influence of the variable viscosity results in lower values of pressure drop for the H boundary condition. The greater distortion of the velocity profile for T(1) relative to the T case causes a higher pressure gradient for the former case. Also, because of the greater distortion of the velocity profile for H(1) than that for H, the pressure drop for the H(1) case is higher than that for the H case.

Effect of viscous dissipation

The effect of viscous dissipation is very important when the viscosity is high or for high shear flows. The Brinkman number is commonly used as a criterion which signifies the relative importance of viscous dissipation.

The effect of viscous dissipation on the temperature profile for different boundary conditions is demonstrated in Figures 8a–d. Also Figures 9a–d show the effect of the Brinkman number on the Nusselt number as well as the dimensionless bulk temperature.

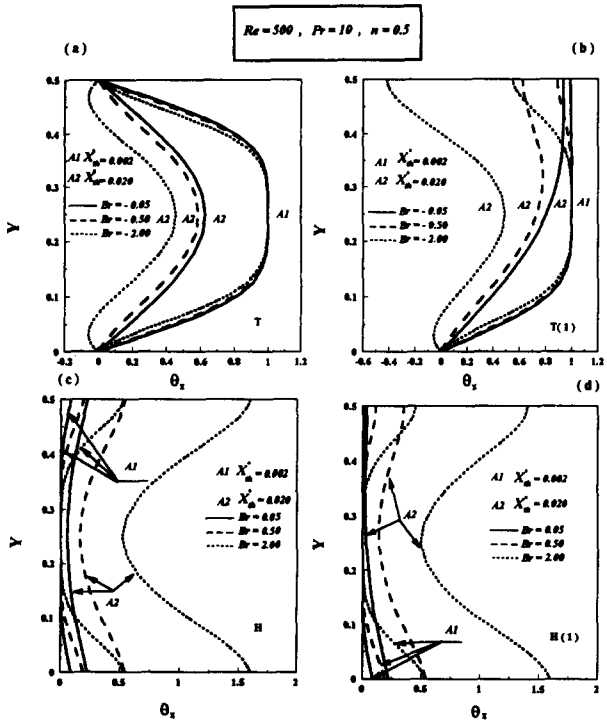

Figure 8(a–d) Effect of viscous dissipation on temperature profiles for different boundary conditions

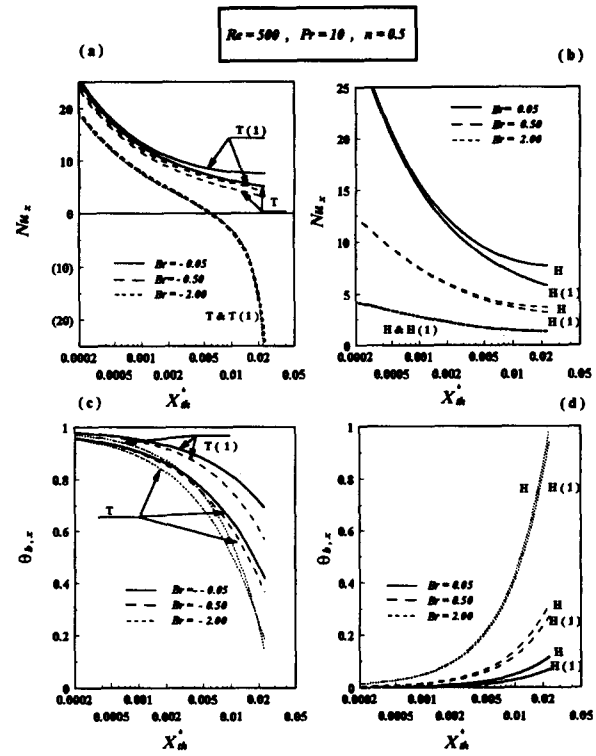

Figure 9(a–d) Effect of viscous dissipation on local Nusselt number and dimensionless bulk temperature for different boundary conditions

First we consider the effect of viscous dissipation for the T and T(1) boundary conditions. For heating, $Br < 0$, whereas the reverse applies for cooling. Because the shear rate is the highest near the wall, the effect of viscous dissipation is most significant in this region. As viscous heating increases the bulk temperature (decreases dimensionless bulk temperature), the local Nusselt number decreases with decreasing Brinkman number. Because of the high temperature difference between wall and fluid in the entrance region, viscous heating has only a slight effect on the Nusselt number. Farther downstream, for low Brinkman numbers, because of combined effects of viscous dissipation and wall heating, the temperature of the fluid close to the wall approximates the wall temperature, so the temperature gradient at the wall is nearly zero; the local Nusselt number also approaches zero. At location farther downstream, the temperature gradient at the wall becomes negative, and the wall temperature is greater than the bulk temperature; this leads to negative values for the local Nusselt number. This indicates reversal in the direction of the heat flux. As the fluid proceeds downstream the fluid bulk temperature increases continuously and finally becomes the same as the wall temperature. Consequently, the Nusselt number becomes infinite. Figures 10a–b show the local Nusselt number, dimensionless bulk temperature and also dimensionless heat flux through the wall for a very long duct (300 times the hydraulic diameter for T boundary condition and $Br = -2$). As shown in this figure far from $X = 0$, $T_{b,x} > T_w$, so the dimensionless bulk temperature is negative. Also because of the negative heat flux in this region the Nusselt number becomes positive again and decreases with the increasing axial distance. At location very far from upstream increases in the dimensionless bulk temperature as well as dimensionless heat flux become very small and the Nusselt number approaches an asymptotic value. Figure 9a indicates that for a specific Brinkman number the asymptotic Nusselt number is lower

than that for the case without viscous dissipation and also the attainment of the asymptotic Nusselt number requires infinitely long duct lengths.

For the T(1) boundary condition and large negative Brinkman numbers, Br = −2.0 (where the viscous heating is dominant), close to the entrance the relative decrease in the Nusselt number $((Nu)_{x,Br=-2.0}/(Nu)_{x,Br=0.0})$ is approximately the same as that for the T boundary condition because of the small effect of viscous dissipation in this region. Farther from the entrance the viscous heating is almost the same for both cases, but because of the greater wall heating in the T boundary condition, the relative decrease in the Nusselt number owing to viscous heating for T(1) is greater than that for T. For Br = −0.05, the dominance of wall heating causes almost the same relative decrease in the Nusselt numbers.

For constant heat flux–type boundary conditions, the Brinkman number is positive for the case of heating. Because the temperature difference between the wall and the fluid is very small in the entrance region, and viscous heating is greater in the inlet region, the most effect of the viscous dissipation is felt in this region. This effect decreases with downstream distance.

Based on the foregoing discussion the viscous heating is a dominant factor in the entrance region for H-type boundary conditions. Thus the relative decrease of the Nusselt number for H and H(1) owing to viscous heating is almost the same in this region, but far from the inlet this decrease for H is greater than that for H(1) boundary condition.

Simultaneous effects of temperature-dependent apparent viscosity and viscous dissipation

When the effect of variable viscosity is considered, the equations of motion and energy are coupled via the temperature-dependent viscosity. The coupling between momentum and energy equations is extended by considering the viscous dissipation effects. When the temperature-dependent viscosity is considered, the velocity profile changes because of heating, and also the viscous heating effect produces higher temperatures in the wall region. The effect of viscous dissipation reduces the heat transfer and also changes the velocity gradient near the wall, which causes increased heat transfer to the fluid.

Table 6 presents the ratio of the Nusselt number for B = 1.5 and Br = −0.5 (or B = −1.5 and Br = 0.5 dependence on the boundary conditions) relative to the case of constant viscosity and no viscous heating. For T-type boundary conditions Table 6 emphasizes the dominant effect of temperature-dependent viscosity close to the entrance because of the fact that the enhancement of the Nusselt number related to variable viscosity is maximal in this region and also the decrement of the Nusselt number because of viscous dissipation is very small. At axial location farther downstream, the viscous

Table 6 Ratio of the Nusselt number for different boundary conditions and Pr = 10, n = 0.5 and Re = 500

X^*_{th}	T	T(1)	H	H(1)
0.0001102	1.086	1.116	0.318	0.321
0.0002927	1.056	1.107	0.386	0.390
0.0004045	1.047	1.098	0.407	0.412
0.0008630	0.993	1.041	0.448	0.456
0.0016512	0.913	0.944	0.472	0.484
0.0032669	0.800	0.818	0.486	0.505
0.0062680	0.684	0.703	0.495	0.526
0.0128136	0.544	0.584	0.515	0.573
0.0221952	0.363	0.419	0.547	0.633

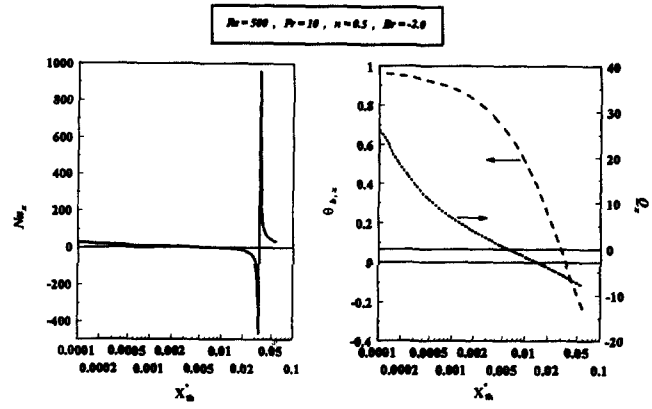

Figure 10(a and b) Local Nusselt number and dimensionless bulk temperature for T boundary condition and Br = −2.0

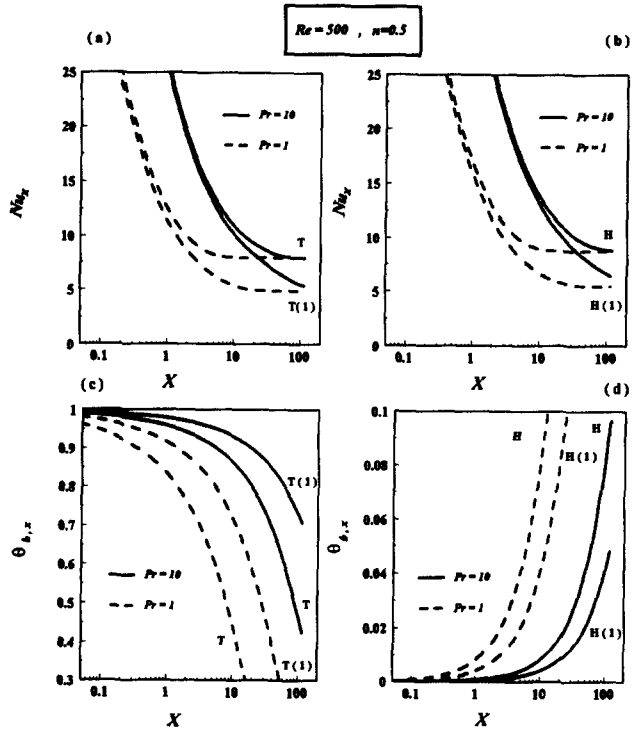

Figure 11(a–d) Effect of Prandtl number on local Nusselt number and dimensionless bulk temperature for different boundary conditions

dissipation effect is dominant and the Nusselt number becomes smaller than that for the case of constant viscosity with no viscous dissipation effects.

For H-type boundary conditions, because the effect of viscous heating is greatest and the variable viscosity effect is small in the entry region, viscous dissipation dominates the Nusselt number distribution in this region.

Effect of Prandtl number

The effect of Prandtl number (defined for a power law fluid, Equation 8) on heat transfer for a fluid of n = 0.5 and different boundary conditions is demonstrated in Figures 11a–d. Nu_x is lower for the lower Prandtl number in the entrance region and asymptotically approaches a value far downstream that is independent of Pr. The lower Prandtl number causes faster thermal development, which results in a higher fluid bulk

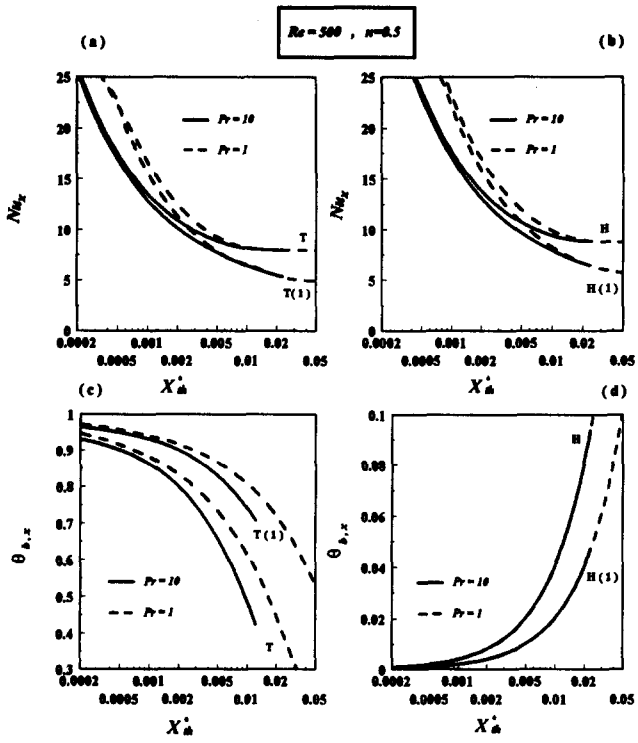

Figure 12(a–d) Effect of Prandtl number on local Nusselt number and dimensionless bulk temperature versus dimensionless axial coordinate for different boundary conditions

temperature (lower dimensionless bulk temperature for the T-type boundary conditions) and also lower dimensionless wall heat flux for T-type boundary conditions. The competition between these two effects causes a lower heat transfer rate. As the fluid proceeds downstream this effect diminishes because of the thermal development. For H-type boundary conditions the lower Pr increases the $(T_{w,x} - T_{b,x})$, which, in turn, results in a lower local Nusselt number.

Figures 12a–d display the effect of Pr on the local Nusselt number and dimensionless bulk temperature versus X^*_{th}. According to this definition of X^*_{th} the lower Prandtl number case results in a higher Nusselt number over the entire length.

Conclusion

A numerical study was carried out of the steady laminar heat transfer for simultaneously developing flow of power law fluids between horizontal parallel plates. The analysis considered the effects of power law index, temperature-dependent viscosity, viscous dissipation, Prandtl number and also the simultaneous effects of variable viscosity and viscous dissipation under a variety of boundary conditions. The favorable comparison of the present results with experimental data available for air as a fluid and also analytical results for fully developed case support the accuracy of these results.

This work has shown that the influence of non-Newtonian behavior on the heat transfer and fluid flow characteristics can be significant. The results are also markedly different from those obtained assuming constant viscosity. Viscosity variation with temperature affects the local Nusselt number and also the pressure drop. For heating, the increase in the local Nusselt number for constant temperature boundary conditions is noticeably higher than that for the constant heat flux boundary conditions.

Viscous heating has a very significant effect on heat transfer, which can even change the direction of heat flux for the case of uniform temperature boundary conditions.

The results indicate that the Prandtl number is a very important parameter; the lower the Prandtl number, the lower the heat transfer in the developing region of the channel.

Acknowledgments

The financial support of Isfahan University of Technology in Islamic Republic of Iran to one of the authors (S. Gh. E.) is gratefully acknowledged.

References

Brinkman, H. C. 1951. Heat effects in capillary flow. *Appl. Sci. Res.*, **A2**, 120

Campos Silva, J. B., Cotta, R. M. and Aparecido, J. B. 1992. Analytical solutions to simultaneously developing laminar flow inside parallel plate channels. *Int. J. Heat Mass Transfer*, **35**, 887–895

Flores, A. F., Gottifredi, J. C., Morales, G. V. and Quiroga, O. D. 1991. Heat transfer to power law fluids flowing in pipes and flat ducts with viscous heat generation. *Chem. Eng. Sci.*, **46**, 1385–1392

Hartnett, J. P. and Kostic, M. 1989. Heat transfer to Newtonian and non-Newtonian fluids in rectangular ducts. *Advances in Heat Transfer*, J. P. Hartnett and T. F. Irvine, Jr. (eds.). 247–356

Hwang, C. L. and Fan, L. T. 1964. Finite difference analysis of forced convection heat transfer in entrance region of a flat rectangular duct. *Appl. Sci. Res.*, **A13**, 401–422

Huhn, J. 1992. Heat transfer in the inlet region of tubes and channels with laminar flow. In *Recent Advances in Heat Transfer*, B. Sunden and A. ZuKauskas (eds.). Elsevier Science, New York, 516–523

Klemp, K., Demmer, T. and Herwing, H. 1992. Entrance flows of non-Newtonian fluids with temperature dependent viscosity. In *Transport Phenomena in Heat and Mass Transfer*, J. A. Reizes (ed.). Elsevier Science, New York, 316–327

Lin, S. H. and Hsu, W. K. 1980. Heat transfer to power law non-Newtonian flow between parallel plates. *Trans. ASME*, **102**, 382–384

Lin, T. 1977. Numerical solutions of heat transfer to yield power law fluids in the entrance region. M.S. thesis, University of Wisconsin, Milwaukee

Lin, T. and Shah, V. L. 1978. Numerical solution of heat transfer to yield power law fluids flowing in the entrance region. *Int. Heat Transfer Conf. 6th. Toronto*, **5**, 317–321

Mercer, W. E., Pearce, W. M. and Hitchcock, J. E. 1967. Laminar forced convection in the entrance region between parallel plates. *J. Heat Transfer*, 251–257

Nguyen, T. V. and Maclaine-Cross, I. L. 1991. Simultaneously developing, laminar flow, forced convection in the entrance region of parallel plates. *J. Heat Transfer*, **113**, 837–842

Patankar, S. V. and Spalding, D. B. 1970. *Heat and Mass Transfer in Boundary Layers*, 2nd ed. Intertext Books, London

Pittman, J. F. 1989. Finite elements for field problems. In *Fundamentals of Computer Modeling for Polymer Processing*, Ch. L. Tucker III, (ed.). Hanser, New York

Rostami, A. A. and Mortazavi, S. S. 1990. Analytical prediction of Nusselt number in a simultaneously developing laminar flow between parallel plates. *Int. J. Heat Fluid Flow*, **11**, 44–47

Shah, R. K. and Bhatti, M. S. 1987. Laminar convection heat transfer in ducts. *Handbook of Single-Phase Convective Heat Transfer* S. Kakac, R. K. Shah and W. Aung (eds.). Wiley, New York, 3.1–3.137

Shah, R. K. and London, A. L. 1978. Laminar flow forced convection in ducts. In *Advances in Heat Transfer*, T. F. Irvine, Jr. and J. P. Hartnett (eds.). Academic Press, New York

Skelland, A. H. P. 1967. *Non Newtonian Flow and Heat Transfer*. Wiley, New York

Yau, J. and Tien, Chi. 1963. Simultaneous development of velocity and temperature profiles for laminar flow of a non Newtonian fluid in the entrance region of flat ducts. *Can. J. Chem. Eng.*, **41**, 139–145

Zienkiewicz, O. C. 1977. *Finite Element Method*. McGraw-Hill, New York